ORIGINAL PAPER

Effects of the geometry and operating temperature on the stability of Ti/IrO$_2$–SnO$_2$–Sb$_2$O$_5$ electrodes for O$_2$ evolution

Xusong Qin · Furong Gao · Guohua Chen

Abstract Ternary IrO$_2$–Sb$_2$O$_5$–SnO$_2$ anode has shown its superiorities over IrO$_2$ and many other electrocatalysts for O$_2$ evolution, in terms of electrochemical stability, activity and cost. The performance of IrO$_2$–Sb$_2$O$_5$–SnO$_2$ anodes is affected by its electrochemical properties and operating conditions. In this paper, the electrochemical stability and activity of the Ti/IrO$_2$–Sb$_2$O$_5$–SnO$_2$ anodes prepared with three different geometries were investigated under different operating conditions. It was found that anodes with large mean curvature have high electrochemical stability. Although increasing temperature results in a decrease in the stability of Ti/IrO$_2$–Sb$_2$O$_5$–SnO$_2$, the anode with a mean curvature of 200 m^{-1} still shows acceptable service life even at 70 °C. This tolerance of high temperature was attributed to the thermal expansion difference between the substrate and the coating layer, the redox window for Ir(V)/Ir(IV) conversion, and the redox reversibility of Sb and Sn species in the coating layer.

Keywords DSA · Electrochemical process ·
Geometry effect · High temperature · Metal oxide anode ·
Service life

1 Introduction

The dimensionally stable anodes (DSAs) invented by Beer in the late 1960s are the most important anodes nowadays in electrochemical engineering. Usually, DSAs use conductive precious metal oxides (RuO$_2$, IrO$_2$, etc.) as electrocatalysts and non-conductive metal oxides (TiO$_2$, Ta$_2$O$_5$, ZrO$_2$, Nb$_2$O$_5$, etc.) as dispersing or stabilizing agents, which are coated on valve metal substrates (Ti, Ta, Zr, W, Nb, Bi) with a thermal decomposition method [1–5]. RuO$_2$ is the most widely used electrocatalyst in DSAs in industry because of its excellent activity for both Cl$_2$ and O$_2$ evolution. However, RuO$_2$ is not stable in acidic environments, and the O$_2$ evolution overpotential increases with time [6, 7]. Several researchers have reported that the electrochemical stability of DSAs can be significantly improved by incorporating other components into RuO$_2$ [8–10]. In spite of significant improvement in electrochemical stability by introducing various components, the durability of RuO$_2$-based DSAs is still insufficient for industrial applications.

In the last two decades, IrO$_2$-based DSAs have received much attention. IrO$_2$ presents a service life about 20 times longer than that of the equivalent RuO$_2$ [11]. Nevertheless, IrO$_2$ is much more expensive than RuO$_2$ and its activity is slightly lower. To save cost and/or to improve the coating property, other components are usually added [12–18]. The stability had been improved significantly for Ti-based ternary IrO$_2$–Sb$_2$O$_5$–SnO$_2$ anode. For example, Chen et al. [19] found that the IrO$_2$–Sb$_2$O$_5$–SnO$_2$ containing 10 mol% of IrO$_2$ has a service life as long as 1600 h under the accelerated life test conditions (3 M H$_2$SO$_4$, 10,000 A m^{-2}, 35 °C). Their investigation also revealed that the optimal calcination temperature is about 550 °C, and both the stability and activity increased as the Ir content increased in the investigated range of 0–10 mol% [20].

In industrial applications, anodes with various geometries may be employed for different electrode systems under different operating conditions. Therefore, the objectives

X. Qin · F. Gao · G. Chen (✉)
Department of Chemical and Biomolecular Engineering,
The Hong Kong University of Science and Technology,
Clear Water Bay, Kowloon, Hong Kong, China
e-mail: kechengh@ust.hk

of the present study were to investigate the effects of operating temperature and substrate geometry on the stability and activity of Ti/IrO$_2$–Sb$_2$O$_5$–SnO$_2$ as anodes for O$_2$ evolution. Interesting results were obtained as discussed subsequently.

2 Experimental section

2.1 Electrode substrate

Titanium disks, titanium rods and titanium cylinders were used as substrates for the preparation of DSA anodes (see Fig. 1). In present study, the Gaussian curvatures of the substrates are identically zero. Therefore, the mean curvatures of the substrates were used to represent the amounts of the three geometrical substrates deviate from being flat. The mean curvature of a flat surface of the titanium surface is zero while the mean curvature for a circular titanium cylinder or rod can be calculated as $H = 1/D$, where D is the diameter of the cylinder or rod. The specifications of the substrates are listed in Table 1.

2.2 Precursor solution preparation

SnCl$_4$·5H$_2$O (98+%, Acros, USA) and SbCl$_3$ (99+%, Acros, USA) were dissolved in iso-propanol (99.7%, Labscan, Thailand) individually, both with a concentration of 0.50 M. Iridium (IV) chloride hydrate (53.89% Ir, Strem Chemicals, USA) was dissolved in the solution made of 1:1 (volume ratio) of iso-propanol and hydrochloric acid (37%, Riedel–deHaen, Germany) also with a concentration of 0.5 M. The solutions underwent an ultrasonic mixing for 1 h to insure all salts were dissolved and distributed uniformly. The precursor solution was then prepared by mixing the individual freshly prepared solutions described

Table 1 Specifications of the titanium substrates

	Diameter (mm)	Thickness or Length (mm)	Effective area (cm^2)	Mean curvature (m^{-1})
Disk	12.5	1	1.2	0
Cylinder	12	5.3	2	83
Rod	5	15	2.6	200

above according to the molar ratio required, namely, Ir:Sb:Sn = 1:1:8.

2.3 Electrodes preparation

All electrodes were prepared by a thermal decomposition method. Prior to coating, the titanium substrates underwent sandblasting, tap water washing, ten minutes of ultrasonic cleaning in deionized water, 2 min of etching in boiling 37% hydrochloric acid, and another ten minutes of ultrasonic cleaning in deionized water. After pretreatment, the titanium substrates were first brushed at room temperature with the precursor solution, dried at 80 °C for 5 min to allow solvents to vaporize, and then baked at 550 °C for 5 min. This procedure was repeated for 18–20 rounds. Finally the electrodes were annealed at 550 °C for 10 h for the sake of stabilizing the active layer. The total oxide loading of the prepared electrodes was around 20 g m^{-2}.

2.4 Accelerated life test

Electrochemical stability is one of the major concerns in an electrochemical process. To evaluate the electrode stability, the accelerated life test was applied here. The test was conducted in a standard three-electrode cell as shown in Fig. 1. The working electrode was mounted on a Teflon holder. Titanium rod (15 mm long and 5 mm in diameter

Fig. 1 The shape of the titanium substrate and schematic diagram of the corresponding three-electrode cell: **a** disk; **b** cylinder; **c** rod
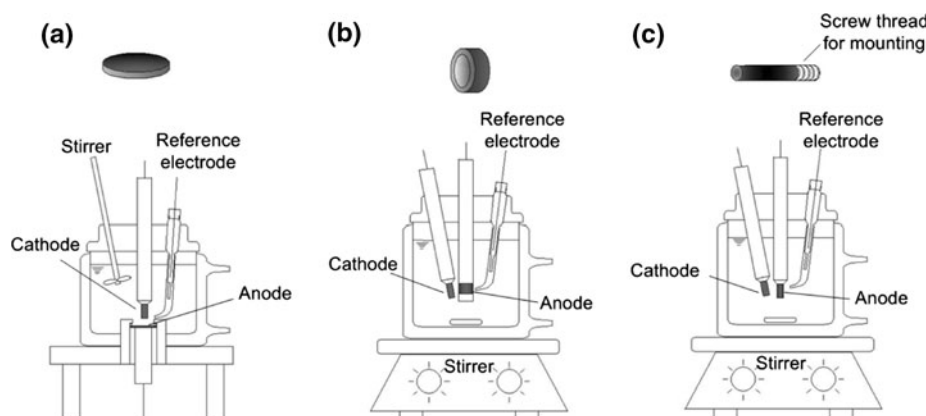
with an effective area of 2.6 cm^2) was also mounted with a Teflon holder as the counter electrode. Ag/AgCl, KCl (sat.) served as the reference electrode. The electrochemical reactors with water jacket were 50 mm in diameter and 70 mm in height for electrodes of disk shape, 80 mm in diameter and 110 mm in height for electrodes of rod or cylinder shape, respectively. The electrolyte was 3 M H$_2$SO$_4$ and the cell temperature was controlled by a water bath (Model 9710, PolyScience Inc, USA). A DC power supply (PD110-5AD, Kenwood, Japan) was used to provide a constant anodic current density of 10,000 A m^{-2}. The potential of the working electrode was periodically monitored and recorded in 5 min interval by a data acquisition and monitoring system. Due to generation of large amounts of bubbles, use of a Luggin capillary was impossible. Because the ohmic drop from the solution was not compensated, the true potential could be a bit smaller than that measured. The working temperature was controlled to be 20, 35 and 70 °C using a water bath. The service life test was taken to be the end at the time when the potential between anode and reference electrode suddenly rose up and exceeded 10 V.

2.5 Physicochemical characterization

Bulk composition in the coating film was examined by Energy-Dispersive Spectrometry plus Scanning Electron Microscopy (EDS-SEM, JSM-6390, JEOL, Japan) and Inductively Coupled Plasma Mass Spectrometry (ICP-MS, Optima 2000, Varian, USA). Surface composition was measured by X-ray Photoelectron Spectroscopy (XPS, PHI 5600, Physical Electronics, USA). Coating microstructure and morphology were analyzed by X-Ray Diffraction (XRD, PW1830, Philips, the Netherlands) and Scanning Electron Microscopy.

2.6 Electrochemical characterization

Electrochemical characterization was performed with a potentiostat/galvanostat (PGSTAT 100, Autolab, The Netherlands) and a standard three-electrode cell (RDE0018, EG&G). Pt wire was used as the counter electrode, and saturated Ag/AgCl, KCl (0.199 V vs. SHE) with a Luggin capillary as the reference electrode. Electrode potentials are quoted with respect to standard hydrogen electrode (SHE). The resistances between the working electrode and the Luggin capillary were measured using the frequency response analyzer of the potentiostat/galvanostat. The ohmic drops of the solutions were compensated. Solutions were purged with nitrogen gas before any electrochemical experiments for about 30 min. Cyclic voltammetry was carried out in 0.5 M H$_2$SO$_4$ and the electrolyte temperature was maintained at 25 °C by a water bath.

3 Results and discussion

3.1 Stability

Ti/IrO$_2$–Sb$_2$O$_5$–SnO$_2$ anodes of different geometries were first subjected to accelerated life tests with different working temperatures to compare their electrochemical stability. Each condition was tested with two replicates. The service lives of the two replicates together with their average value are shown in Fig. 2. Here, the upper bound, lower bound and the circle marker at a given condition represent the maximum, minimum service lives and their average value, respectively.

Two phenomena can be observed from Fig. 2. First, the working temperature significantly affected the service life of Ti/IrO$_2$–Sb$_2$O$_5$–SnO$_2$ anodes. When the temperature was increased from 20 to 70 °C, the average accelerated service lives of the replicates accordingly decreased from 1258, 802 and 131 h to 263, 133 and 4.5 h for anodes with titanium rod, cylinder and disk substrates, respectively. In other words, the stability of the anodes with titanium rod, cylinder and disk substrates decreased 80, 83 and 97% while the working temperature was increased from 20 to 70 °C. Second, the effect of the anode geometries is quite significant in affecting its durability. For example, under the same high temperature of 70 °C, it is seen that the service life of the disk shape anode with a zero mean curvature only had a value about 4.5 h which is clearly not a stable type of electrode under this condition. However, the rod shaped electrode of a mean curvature of 200 m^{-1} operated 263 h before its failure. This value would mean a working life to be over 10 years when the current density is lowered to 300 A m^{-2} in a neutral solution for O$_2$
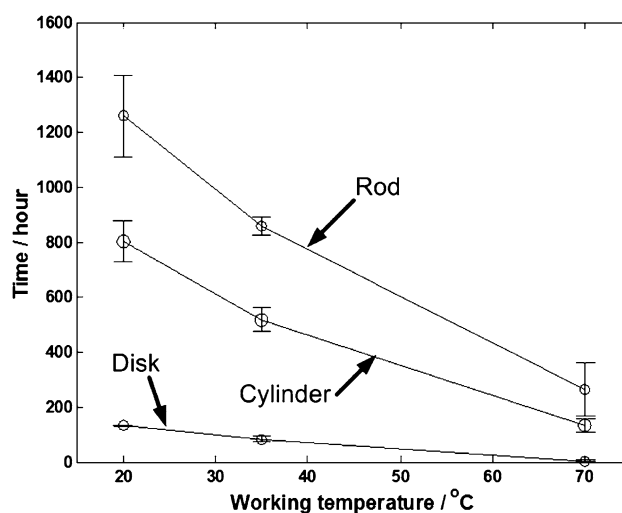
Fig. 2 Service life comparison of Ti/IrO$_2$–Sb$_2$O$_5$–SnO$_2$ with different geometrical substrates in 3 M H$_2$SO$_4$ solution under 10,000 A m^{-2} at different working temperature

evolution according to the method of estimation in literature [20, 21].

The higher the working temperature, the shorter the service life of an electrode is an expected phenomenon. The increased temperature would accelerate the rate of the dissolving of the active layer of metal oxides, enhance the rate of the penetration and the electrolytes across the coating and the passivation of the substrate. The chemical reaction for O_2 evolution may also take place at a level deeper inside the coating layer [22]. Of course, the mismatch of the thermal expansion coefficient between the coating layer and the substrate material is always the source of service life deterioration when there are temperature changes involved. This may be one of the reasons why there is a significant effect of the electrode geometry on its stability. With higher mean curvature, the radial expansion of the titanium substrate will be less and provide better adhesion of the oxide coating at high temperature, compared with lower mean curvature substrates. The titanium substrate is then well covered by the oxide coating, preventing the direct contact between the titanium substrate and the electrolyte during electrolysis. The oxidation of the titanium substrate will be restrained and the electrochemical stability of DSAs is accordingly improved.

Other two possible reasons may be the coating thickness and composition differences among ternary IrO_2–Sb_2O_5–SnO_2 coating on the various geometric substrates. Although the starting precursor solution is of the same

composition and the same number of paintings on the substrates was performed, because of their geometrical differences, the final coating thickness and composition of the coating layer would be quite different, as discussed in the following section. In present study, the thickness of the oxide layer is about 3 μm examined by SEM. This value was also confirmed by EDS results since the Ti species were detected in EDS results. However, because examining the thickness of the oxide film using SEM would need to cut the electrodes, it is impossible to test its life time after SEM study. Therefore, the total oxide coating loading is used to represent the thickness of the thin film. In present study the total oxide coating loadings of anodes with disk, cylinder and rod titanium substrates are 21.3 ± 2.4, 18.4 ± 4.2 and 18.3 ± 0.9 g m^{-2}, respectively. The thickness of the coating layer is proportional to total oxide loading. Thus, for the three geometries tested, the coating layer thickness should not differ too much. It is also interesting to note that the disk-shaped electrode should have the thickest coating but had the shortest service life. This finding indicates that the coating thickness is not a major factor influencing the service life of electrodes tested in the present study.

3.2 Coating composition

The coating composition of Ti/IrO_2–Sb_2O_5–SnO_2 electrode was analyzed by XPS, EDS and ICP-MS. Actually, the

Fig. 3 XPS spectra of IrO_2–Sb_2O_5–SnO_2 film coated on titanium: a disk; b cylinder; c rod substrates
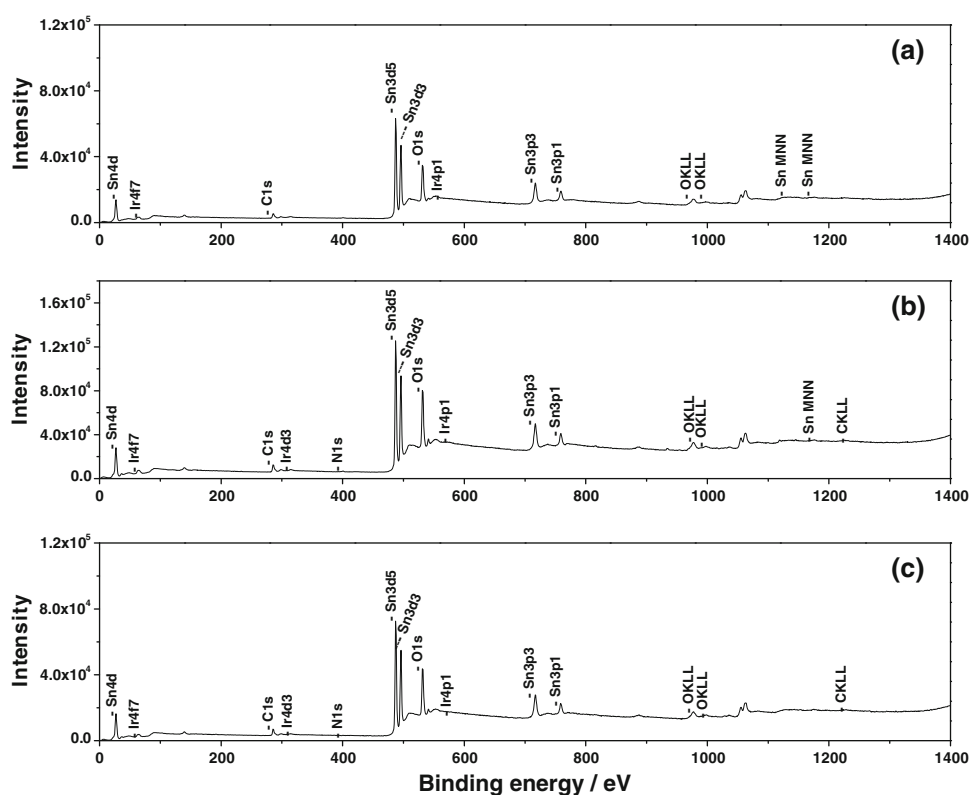
Table 2 Coating compositions of IrO_2–Sb_2O_5–SnO_2 film measured by EDS and XPS

Element	Atomic concentration (%)					
	XPS			EDS		
	Disk	Cylinder	Rod	Disk	Cylinder	Rod
Ir	0.87	1.09	0.98	2.30	1.63	1.82
Sb	1.07	1.19	0.54	0.67	0.62	0.37
Sn	21.1	20.1	22.4	13.6	8.50	13.5
C	18.0	17.6	18.8	4.59	2.58	5.52
O	59.0	60.3	57.3	78.3	86.5	78.8
Cl	0	0	0	0	0	0
Ti	0	0	0	0.53	0.2	0.03

maximum sampling depth of XPS is only 50–80 nm. Therefore, the XPS analysis results represent the elemental concentrations at the coating surface. EDS is usually used to measure the bulk elemental concentrations in a film. Its maximum sampling depth is about 3 μm. But EDS can only examine a limited coating area due the orientation of the electrode and the position of the electronic probe of the EDS-SEM machine. Thus, ICP-MS was employed to measure the composition of the dissolved film from the electrode.

Figure 3 shows the XPS spectra of IrO_2–Sb_2O_5–SnO_2 films coated on various titanium substrates. The atomic concentrations of IrO_2–Sb_2O_5–SnO_2 coating measured by XPS and EDS are shown in Table 2.

No Cl^- signals were observed in the XPS spectra and EDS analysis results, implying all the Cl's were substituted by oxygen in the oxide lattices. The facts that no Ti signal was detected by XPS and only a small amount of Ti was detected by EDS indicate that the titanium substrates were well covered by IrO_2–Sb_2O_5–SnO_2 coatings and the coating thicknesses are about 3 μm. The detected carbon in XPS and EDS results could be attributed to adsorption of carbon impurities (e.g. carbon dioxide or oil from vacuum pumps) on the coating surface, or to the C content in the solvents. The IrO_2 content in the IrO_2–Sb_2O_5–SnO_2 coating surface (XPS) on titanium disk, cylinder and rod substrates are 3.78, 4.88 and 4.10 mol%, respectively. However, the

values in bulk (EDS) are 13.85, 15.16 and 11.62 mol%, respectively. These much higher than 10% Ir values may imply the lack of accuracy of EDS in quantitatively measuring light elements.

ICP-MS analysis provides more accurate bulk Ir/Sb/Sn molar ratio of the electrode coating film as shown in Table 3. The very high concentrations of Ti indicate the complete dissolution of the coatings. The Ir:Sb:Sn ratios of the coating films measured on titanium disk, cylinder and rod substrates are 1.09:1:15.4, 3.48:1:53.9 and 6.8:1:133, respectively, which are quite different from the precursor solution, 1:1:8. The extreme low concentrations of Sb in the coating films were attributed to the low decomposition temperature of Sb_2O_5, 380 °C, and overly long annealing time at the high temperature. The IrO_2 content in the IrO_2–Sb_2O_5–SnO_2 coating films coated on titanium disk, cylinder and rod substrates are 6.24, 5.96 and 4.84 mol%, respectively, which are closed to the XPS analysis results. The different yields of IrO_2, Sb_2O_5, SnO_2 on these three geometric substrates could be expected because the thermal decomposition method applied in present study is very sensitive to the geometry of the sample, solvent used, the concentration and the nature of the metal salts, as discussed in [23]. Nevertheless, it is quite interesting that the Ti/IrO_2–Sb_2O_5–SnO_2 electrode with titanium rod substrate has the least Sb and Ir contents, but the longest service life. The relationship between the composition and the service life needs further study to explain.

3.3 Coating crystal structure

Figure 4 shows the XRD patterns of the IrO_2–Sb_2O_5–SnO_2 film coated on titanium disk, cylinder and rod substrates at a scan speed of $0.002°$ s^{-1}, with the current and voltage of the X-ray source as 40 mA and 40 kV, respectively. In addition to the Ti metal peaks from the substrates, only a single set of broad and symmetric peaks corresponding to the rutile structure with peak positions deviating from the pure SnO_2 was found in all the Ti/IrO_2–Sb_2O_5–SnO_2 electrodes. Neither IrO_2-rich peaks nor Sb_2O_5-rich peaks were detected in present study. These facts reveal that various components in the IrO_2–Sb_2O_5–SnO_2 have been highly intermixed. In other words, IrO_2–Sb_2O_5–SnO_2

Table 3 Coating compositions of IrO_2–Sb_2O_5–SnO_2 film measured by ICP-MS

	Concentration in HCl solution (mg L^{-1})				Ir/Sb/Sn concentration in ternary metal solid solution (mol%)		
	Ti	Sn	Sb	Ir	Sn	Sb	Ir
Disk	1240	6.01	0.4	0.69	88.0	5.71	6.24
Cylinder	3010	20.0	0.38	2.09	92.3	1.71	5.96
Rod	3670	15.6	0.12	1.29	94.5	0.71	4.84

Fig. 4 XRD spectra of IrO$_2$–Sb$_2$O$_5$–SnO$_2$ film coated on titanium: **a** disk; **b** cylinder; **c** rod substrates at a scan speed of 0.002° s^{-1}
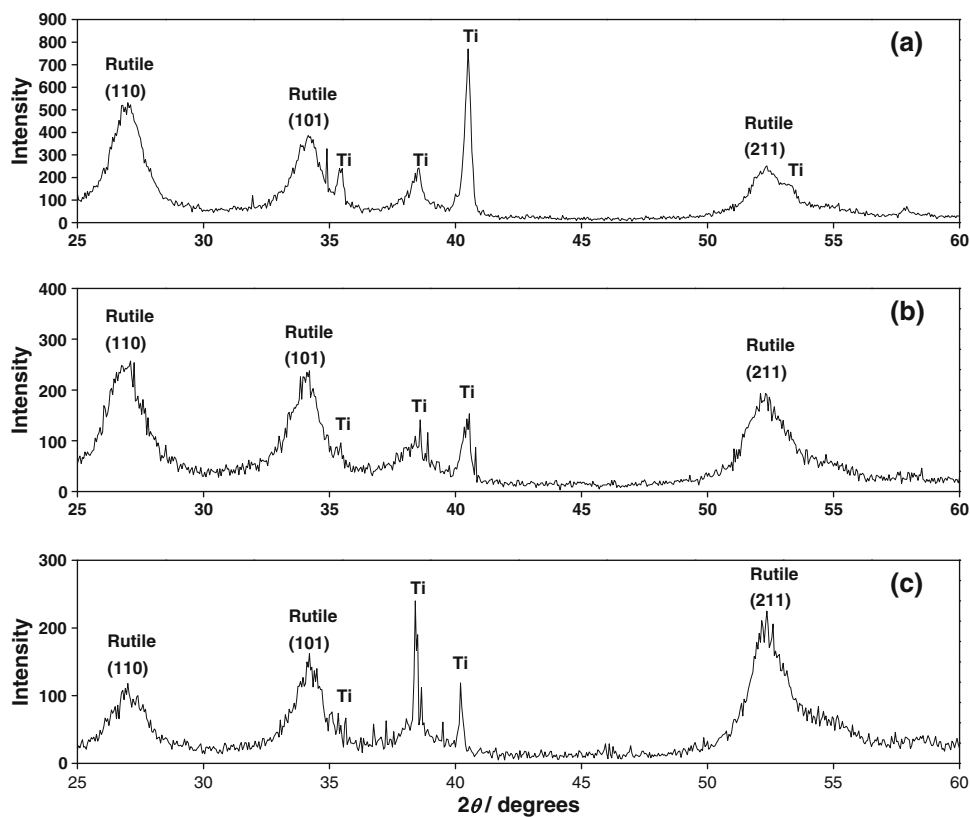
Fig. 5 SEM images of IrO$_2$–Sb$_2$O$_5$–SnO$_2$ film coated on titanium: **a** disk; **b** cylinder; **c** rod substrates
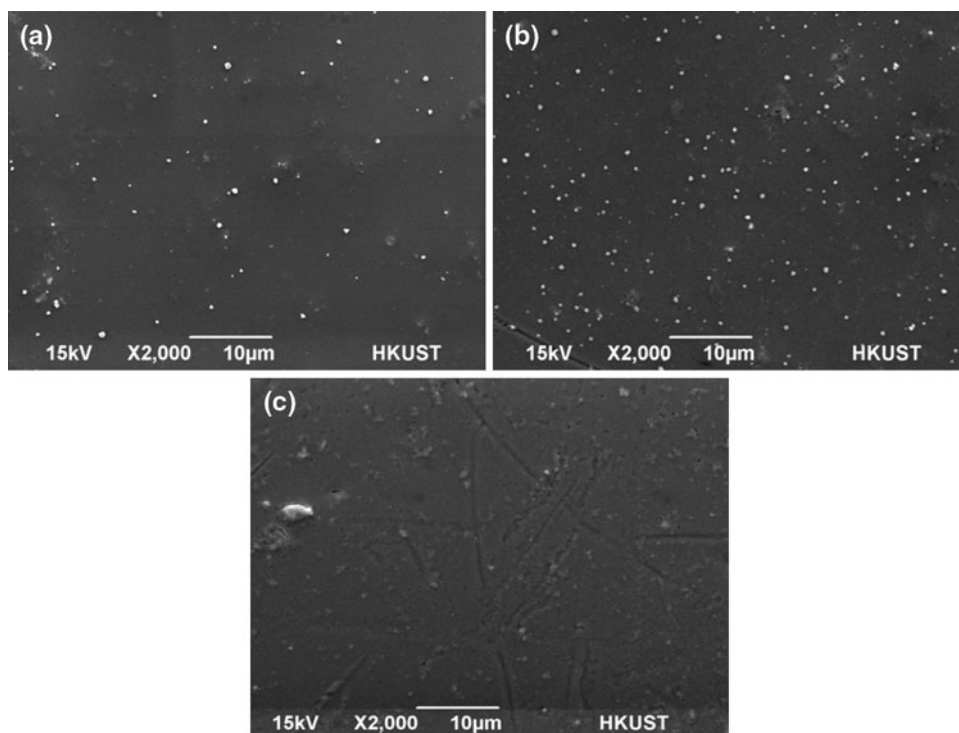
exists in the form of a solid solution on all these electrodes. These XRD results are consistent with previous studies [19, 20]. There are noticeable differences among the IrO$_2$–Sb$_2$O$_5$–SnO$_2$ coating films in terms of the peak intensity.

These intensity differences can be explained by the effect of the substrate geometry since the interaction between X-ray beam and the sample would be larger if the sample surface is flatter.

3.4 Surface morphology

Figure 5 shows the typical SEM images of IrO_2–Sb_2O_5–SnO_2 coating films coated on titanium disk, cylinder and rod substrates. The IrO_2–Sb_2O_5–SnO_2 film on disk substrate is quite compact and smooth, with cracks or pores rarely observed. In contrast, more cracks and pores can be found on the coating surfaces on titanium cylinder or rod substrates. The white spots seen for all the electrodes probably belong to the amorphous constituents.

3.5 Electrochemical characterization

Figure 6 shows the cyclic voltammograms obtained on Ti/IrO_2–Sb_2O_5–SnO_2 electrodes with three different geometrical substrates in 0.5 M H_2SO_4 solution. The cyclic voltammograms obtained in present study are consistent with the literature, with respects to the shape, and convergence rate of the cyclic voltammograms in spite of the substrate geometry differences [24]. This is attributed to the extremely high electrochemical stability of Ti/IrO_2–Sb_2O_5–SnO_2.

During potential scan, the oxidation states of iridium may change, and thus well-defined current peaks can usually be identified on IrO_x coated electrodes. Huppauff and Lengeler [25] clearly observed the anodic and cathodic peaks from the redox-couples of Ir(III)/Ir(IV) and Ir(IV)/Ir(V) on IrO_x films deposited on glass substrates. But Mousty et al. [26] could only detect the anodic and cathodic peaks from Ir(III)/Ir(IV) and the cathodic peak from Ir(IV)/Ir(V) on the Ti/IrO_x electrode prepared by induction heating, whereas the anodic peak from Ir(IV)/Ir(V) was hardly noticeable. In our precious study of the electrochemical behaviour of Ti/IrO_2–Sb_2O_5–SnO_2 anodes [24], only a very broad cathodic current peak at around 0.90 V and 1.35 V of Ir(IV) to Ir(III), and Ir(V) to Ir(IV) and a very week anodic current peak at about 1.35 V of Ir(III) to Ir(IV), and Ir(IV) to Ir(V) for the Ti/IrO_2–Sb_2O_5–SnO_2 electrode were found. In another study [27], a clear cathodic current peak at about 1.35 V and an anodic current peak at about 1.4 V could be observed. According to reference [24, 25, 27], these two peaks are corresponding to the Ir(IV) to Ir(V) redox transition.
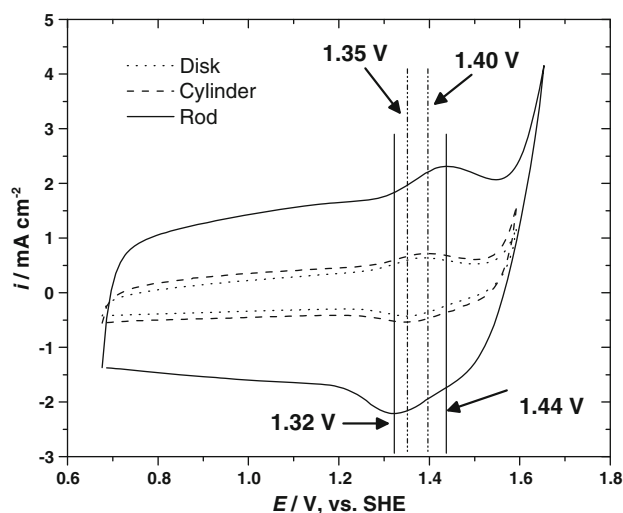
In present study, the upper potential limits were extended to 1.59, 1.59 and 1.65 V for disk, cylinder and rod shaped Ti/IrO_2–Sb_2O_5–SnO_2 anodes, respectively. Clear cathodic and anodic peaks can be found in Figs. 6 and 7. The cathodic and anodic peaks of three Ti/IrO_2–Sb_2O_5–SnO_2 electrodes with titanium disk and cylinder substrates were found at 1.35 V and 1.4 V which are consistent with reference [26]. However, the cathodic and anodic peak positions of Ti/IrO_2–Sb_2O_5–SnO_2 electrode with rod substrate differed from above results. Its cathodic and anodic
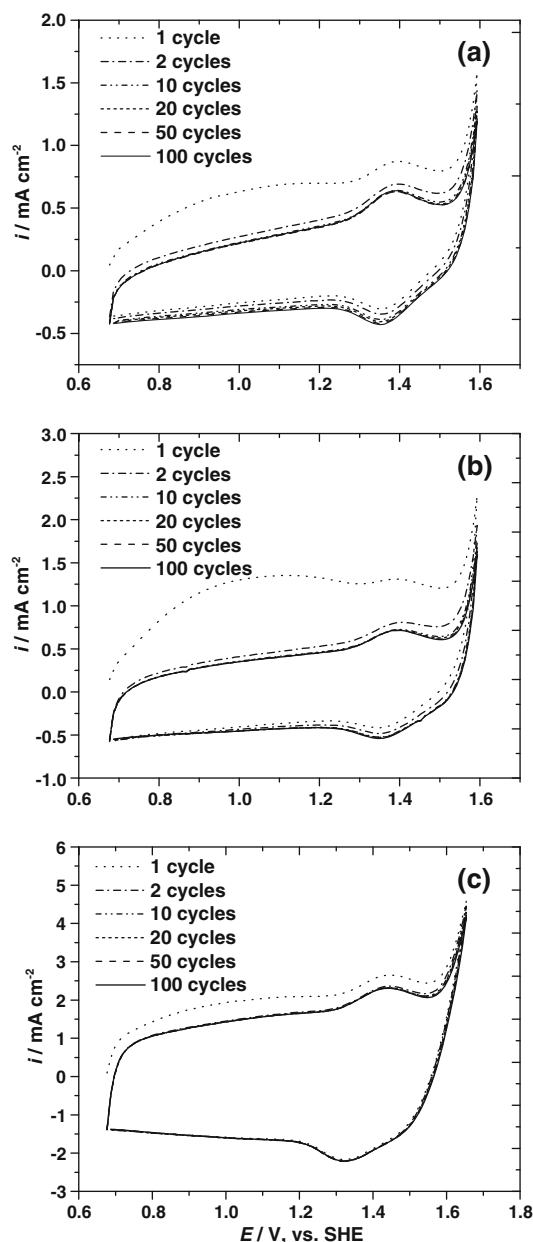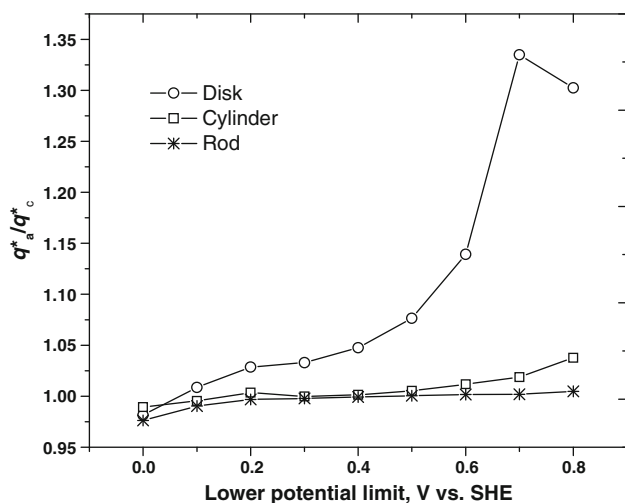

Fig. 6 Cyclic voltammograms with cycles of IrO_2–Sb_2O_5–SnO_2 film in 0.5 M H_2SO_4 at a scan rate of 100 mV s^{-1}: **a** disk; **b** cylinder; **c** rod substrates

peaks were found at 1.32 V of Ir(V) to Ir(IV) and 1.44 V of Ir(IV) to Ir(V), respectively. The potential window between the cathodic and anodic peaks was therefore 0.12 V, which is much bigger than the cases of the electrodes with titanium disk or cylinder substrates, say 0.05 V. The bigger redox potential window is associated with higher electrochemical stability, as discussed in previous sections.

As the potential scan limit is extended to the lower potential region, the redox reactions of Sb(III)/Sb(V) and Sn(II)/Sn(IV) occurred. Voltammetric studies were conducted in present study to investigate the reversibility of

Fig. 7 Comparison of 100th cycle of cyclic voltammograms of IrO_2–Sb_2O_5–SnO_2 film in 0.5 M H_2SO_4 at a scan rate of 100 mV s^{-1}

Fig. 8 Dependence of anodic-to-cathodic voltammetric charge ratio on lower potential limit at a fixed upper potential limit of 1.20 V vs. SHE

conversion of Sb and Sn species coated on larger mean curvature substrates in high potential region is stronger than on the smaller mean curvature titanium substrates. This may also partially explain the better stability of the anodes of larger mean curvature.

4 Conclusions

Operating temperature and substrate geometry could affect the stability and activity of Ti/IrO_2–Sb_2O_5–SnO_2 electrode significantly. The service life of Ti/IrO_2–Sb_2O_5–SnO_2 electrode decreases significantly as operating temperature increases. The anodes prepared with larger mean curvature substrates were found to have longer service lives although their coating films had some pores and cracks, and were not as compact as the ones prepared with smaller mean curvature substrates. For the anode with a mean curvature of 200 m^{-1}, an accelerated life of 263 h was obtained which can be projected to be over 10 years under 300 A m^{-2}. The relationship between the substrate geometry and the stability of the anode for O_2 evolution may be explained by the thermal expansion difference between the substrate and the coating layer, the redox window for Ir(V)/Ir(IV) conversion, and the redox reversibility of Sb and Sn species in the coating layer.

References

1. Beer HB, Hinden JM (1982) USA patent 4331528
2. Beer HB (1972) USA patent 3632498
3. Beer HB (1973) USA patent 3771385
4. Beer HB (1980) J Electrochem Soc 127:303C
5. Novak DM, Tilak BV, Conway BE (1982) In: Bockris JO, Conway BE, White RE (eds) Modern aspects of electrochemistry. Plenum Press, New York, pp 195–318
6. Burke LD, Murphy OJ, O'Neill JF, Venkatesan S (1977) J Chem Soc Faraday Trans 73:1659
7. Loucka T (1977) J Appl Electrochem 7:211
8. Burke LD, McCarthy M (1984) Eletrochim Acta 29:211
9. Iwakura C, Sakamoto K (1985) J Electrochem Soc 132:2420
10. Chen X, Chen G (2005) Electrochim Acta 50:4155
11. Alves VA, Silva LAD, Oliveira ED, Boodts JFC (1998) Mater Sci Forum 655:289
12. Stucki S, Muller R (1981) In: Veziroglu TN, Fueki K, Ohta T (eds) Hydrogen energy progress (Proceedings of the 3rd world hydrogen energy conference, Tokyo, 1980), Pergamon Press, Oxford
13. Hutchings R, Muller K, Kotz F, Stucki S (1984) J Mater Sci 19:3987
14. Rolewicz J, Comninellis Ch, Plattner E, Hinden J (1988) Electrochim Acta 33:573
15. Comninellis Ch, Vercesi GP (1991) J Appl Electrochem 21:335
16. Vercesi GP, Rolewicz F, Comninellis Ch (1991) Electrochim Acta 176:31
17. Balko EN, Nguyen PH (1991) J Appl Electrochem 21:678

the conversion of Sb and Sn species, by fixing the upper potential limit at 1.2 V and decreasing the lower potential limit from 0.8 to 0 V in a step of 0.10 V. The voltammograms of the DSAs with various geometric substrates obtained in this study are consistent with reference [24]. However, the anodic-to-cathodic voltammetric charge ratios at different potential scan ranges, q_a^*/q_c^*, show significant differences among the DSAs (see Fig. 8). For the anode with titanium disk substrate, q_a^*/q_c^* drops from 1.30 to 0.98 as the lower potential limit decreases from 0.8 to 0 V. This q_a^*/q_c^* variation is much larger than those q_a^*/q_c^* variations of the anodes with titanium cylinder and rod substrates, indicating that the reversibility of the

18. Cardarelli F, Taxil P, Savall A, Comninellis Ch, Manoli G, Leclerc OJ (1998) J Appl Electrochem 28:245
19. Chen X, Chen G, Yue PL (2001) J Phys Chem B 105:4623
20. Chen X, Chen G (2005) J Electrochem Soc 152:J59
21. Hine F, Yasuda M, Noda T, Yoshida T, Okuda J (1979) J Electrochem Soc 126:1439
22. Fierro S, Nagel T, Baltruschat H, Comninellis Ch (2007) Electrochem Comm 9:1969
23. Comninellis Ch, Vercesi GP (1991) J Appl Electrochem 21:136
24. Chen G, Chen X, Yue PL (2002) J Phys Chem B 106:4364
25. Huppauff M, Lengeler BJ (1993) Electrochem Soc 140:598
26. Mousty C, Foti G, Comninellis Ch, Reid V (1999) Electrochim Acta 45:451
27. Chen X, Chen G, Yue PL (2002) Environ Sci Technol 36:778